# High-Performance Biosensing Systems Based on Various Nanomaterials as Signal Transducers

Review

**Title: High-performance biosensing systems based on various nanomaterials as signal transducers**

Jaewook Lee[1]

Oluwasesan Adegoke[1]†

Enoch Y. Park[1,2,3]

[1]*Laboratory of Biotechnology, Research Institute of Green Science and Technology, Shizuoka University, 836 Ohya, Suruga-ku, Shizuoka 422-8529, Japan*

[2]*Laboratory of Biotechnology, Department of Bioscience, Graduate School of Science and Technology, Shizuoka University, 836 Ohya, Suruga-ku, Shizuoka 422-8529, Japan*

[3]*Laboratory of Biotechnology, College of Agriculture, Academic Institute, Shizuoka University, 836 Ohya, Suruga-ku, Shizuoka 422-8529, Japan*

**Correspondence:** Enoch Y. Park*, Laboratory of Biotechnology, Research Institute of Green Science and Technology, Shizuoka University, 836 Ohya, Suruga-ku, Shizuoka 422-8529, Japan.* **E-mail**: *park.enoch@shizuoka.ac.jp*

† Present affiliation: Leverhulme Research Centre for Forensic Science, University of Dundee

**Keywords:** Biosensor; Carbon nanomaterial-based biosensor; Electrical biosensor; Nanoparticle-based biosensing system; Optical biosensing platform

**Abbreviations: MeNP,** metal nanoparticle; **QD,** quantum dot; **MNP,** magnetic nanoparticle; **CNM**, carbon nanomaterial; **CNT**, carbon nanotube; **GRP**, graphene; **SERS**, surface-enhanced Raman scattering; **PRET**, plasmonic resonance energy transfer; **FRET**, fluorescence resonance

energy transfer; **MO**, magneto-optical; **LSPR**, localized surface plasmon resonance; **Abs**, absorbance; **LOD**, limit of detection; **aG**, Antigen; **aB**, Antibody; **TB**, tuberculosis; **ELISA**, enzyme-linked immunosorbent assay; **HRP**, horseradish peroxidase; **TMB**, 3,3',5,5'-tetramethylbenzidine; **TMB$_{ox}$**, oxidized TMB; **FI**, fluoroimmunoassay; **u-Au NPs**, urchin-like Au NPs; **DI**, deionized; **MB**, molecular beacon; **MeNP-GRP**, MeNP-decorated GRP; **MeNP-CNT**, MeNP-decorated CNT; **EDC/NHS**, ethyl(dimethylaminopropyl) carbodiimide/N-hydroxysuccinimide; **CdTe**, Cadmium telluride; **UCNPs**, upconversion nanoparticles; **CEA**, carcinoembryonic antigen; **CNP**, carbon nanoparticle; **PAA**, poly acrylic acid; **NoV-LPs**, norovirus-like particles; **IDE**, interdigitated electrode; **MWCNT**, multiwalled CNT; **GCE**, glassy carbon electrode; **DPV**, differential pulse voltammetry

**Abstract**

Recently, highly sensitive and selective biosensors have become necessary for improving public health and well-being. To fulfill this need, high-performance biosensing systems based on various nanomaterials, such as nanoparticles, carbon nanomaterials, and hybrid nanomaterials, have been developed. Numerous nanomaterials have shown excellent physical properties, including plasmonic, magnetic, catalytic, mechanical and fluorescence properties and high electrical conductivities, and these unique and beneficial properties have contributed to the fabrication of high-performance biosensors with various applications, including in optical, electrical, and electrochemical detection platforms. In addition, these properties could be transformed to signals for the detection of biomolecules. In this review, various types of nanomaterial-based biosensors were introduced, and they showed high sensitivity and selectivity. In addition, the potential applications of these sensors on the biosensing of several types of biomolecules were also discussed. These nanomaterials-based biosensing systems have provided a significant improvement on healthcare including rapid monitoring and early detection of infectious disease for public health.

# 1. Introduction

An increase in the social awareness, interest in health care and public safety issue, recently, highly sensitive and selective biosensing systems have been required [1, 2]. In addition, fast detection systems are desired to prevent the spread of contagious diseases [3]. To meet these kinds of critical requirements, several types of high-performance virus detection platforms have been developed using many nanomaterials that possess unique and multifunctional properties [4-8].

Several nanomaterials have been developed and introduced, such as metal nanoparticle (MeNP), quantum dot (QD), magnetic nanoparticle (MNP), and carbon nanomaterial (CNM), which include carbon nanotube (CNT), graphene (GRP), and GRP-QD [9-13]. These nanomaterials have unique properties, such as optical, plasmonic, fluorescence, magnetic, mechanical and catalytic properties and a high electrical conductivity [14-16]. On the other hand, hybrid nanomaterials, including core/shell or alloyed nanoparticles and nanoparticle-modified carbon nanomaterials, have shown excellent synergistic effects, such as surface-enhanced Raman scattering (SERS), plasmonic resonance energy transfer (PRET), fluorescence resonance energy transfer (FRET), magneto-optical (MO) effects, enhanced catalytic properties, enhanced electrical conductivity and improved mechanical properties [17-20]. In sensing system, these properties of nanomaterials are key to their function as signal transducers, in which interactions between a certain nanomaterial and a target virus induce changes in the properties of the nanomaterial property, resulting in the detection of a specific target virus.

Due to these unique properties, numerous nanomaterials have contributed to the construction of platforms for the detection of viruses, DNA, RNA and critical diseases with various approaches [21-23]. MeNPs, QDs and MNPs have been utilized in optical and electrochemical sensing platforms [24-26], and carbon nanomaterials have been used in electrical and optical detection systems [27-29]. Hybrid nanomaterials have also been applied in various sensing systems [30-32], and these nanomaterials can potentially assist in the development of on-site or point-of-care monitoring systems [33].

In this review, various nanomaterial-based high-performance biosensing systems and the types of nanomaterial properties that can be adopted as signal transducers for the detection of biomolecules and viruses are introduced.

## 2. Plasmonic and catalytic nanoparticle-based biosensing systems

Noble MeNPs such as Au, Ag and Pt NPs have unique optical properties that are characterized by a strong plasmonic absorbance (Abs) at a specific wavelength, which originates from the localized surface plasmon resonance (LSPR) effect [34-36]. The wavelength of this plasmonic absorbance can be tuned through self-assembly processes and the resulting plasmonic coupling interactions [37-39], and many researchers have the modulated plasmonic properties via structural alteration of Au or Ag NPs with biomolecules, such as peptides, proteins, and DNA [40-44]. This tuning ability indicates that the plasmonic absorbance can be used as a signal transducer for the biosensing of target biomolecules because its wavelength changes with the biomolecule-induced self-assembly of MeNPs [45, 46].

Zhang *et al.* detected target DNA by controlling the plasmonic properties of Au NPs using probe DNA-modified Au NPs [47]. To capture the target DNA, two different types of DNA probes were respectively introduced on large (40 nm) and small Au NPs (17 nm). In this case, the probes played the roles of a plasmonic core and satellite for achieving plasmonic coupling interactions. If the target DNA was present in the system, the plasmonic core and satellite spontaneously assembled through DNA hybridization as shown in Figure 1A.

After the DNA-mediated assembly process, plasmonic interactions occurred between the core and satellite, and as a result, the $\lambda_{max}$ of the plasmonic absorbance spectrum redshifted. According to Figure 1B, the $\lambda_{max}$ redshifted from 521 nm to 582 nm after the target DNA mediated-assembly process. As shown in Figure 1C and D, before reaction, a single core was observed by SEM, whereas after reaction, many satellites were observed around a single core. In addition, as the concentration of target DNA increased from 0 to 1000 nM, the $\lambda_{max}$ of the core-satellite structure redshifted further and saturated at approximately 100 nM target DNA because

of the capacitance of the core Au NP. This result also indicated that the number of satellite Au NP was controlled by the concentration of target DNA. Interestingly, this system could be reused following a DNA dissociation process performed by increasing the temperature. Additionally, Gao *et al.* demonstrated the detection of target DNA via monitoring of the plasmonic coupling interactions that occurred with the DNA hybridization-induced assembly of Au NPs [48]. In this case, two different types of probe DNA-modified Au NPs dimerized to form a Y-shaped DNA duplex structure between the probe DNAs and target DNA (Figure 1E). Depending on the concentration of target DNA, the plasmonic coupling interactions in the Au dimer structure also changed, and as a result, a secondary plasmonic absorbance band appeared at approximately 600 nm (Figure 1F). As the concentration of target DNA increased, the absorbance of the secondary plasmon resonance also linearly increased, and the limit of detection (LOD) was estimated to be approximately sub-pM (Figure 1G). The target DNA mediated-Au NP dimer structure was clearly observed by using SEM and is depicted in Figure 1H.

The change in the plasmonic absorbance could also be one of the measurement factors in the detection of a virus or DNA. In this case, a magnetophoretic immunoassay was introduced to demonstrate the efficacy of the detection system [33, 49, 50]. For example, Kim *et al.* detected tuberculosis (TB) aG (CFP-10) using Au NPs and MNPs [51]. In this study, the surface of each NP was modified with a TB-specific antibody (aB) to capture CFP-10 TB aG (Figure 2A). When the target aG was present in the NP mixture, a sandwich structure formed between an Au NP and an MNP through a key and lock reaction. During the magnetophoresis process, the aG-mediated hybrid structures moved toward a magnet, and the Au NPs were ultimately removed from the mixture (from 1 to 3 of Figure 2B). In other words, the concentration of Au NPs in the mixture decreased, and the change in the intensity of the plasmonic absorbance was measured as a function of the target aG concentration. In Figure 2C, the time course of the plasmonic absorbance is shown for CFP-10 concentrations from 10 pg/ml to $10^4$ pg/ml; as the concentration of CFP-10 increased, a decrease in the absorbance was observed. Moreover, this magnetophoresis immunoassay showed a fast response, as the entire detection process was completed within 400 sec.

6

Additionally, a highly sensitive detection performance was exhibited, and a linear calibration curve was obtained using the collected plasmonic absorbance at 525 nm in the presence of various concentrations of CFP-10. The $\Delta$Abs ($Abs_{immune} - Abs_{control}$) was calculated to estimate the difference in the plasmonic intensity before and after the magnetophoresis immunoassay, and based on the calibration curve, the LOD of this sensing system was estimated to be approximately 10 pg/ml (Figure 2D). In addition, excellent selectivity against other types of aG and biomolecules was observed for this system. In another case, target DNA was detected by a magnetophoresis immunoassay based on the change in the plasmonic absorbance.

The catalytic and enzymatic properties of NP-based biosensing platforms have also been highlighted due to their rapid sensing process, visualization by the naked eye and high sensitivity [52-56]. In particular, since MeNPs possess enzyme-like activities, they can be utilized in the place of an enzyme in an enzyme-linked immunosorbent assay (ELISA) to catalyze and activate the visualization reagent [57-59]. Ahmed *et al.* reported the detection of the influenza virus (H1N1) through the catalytic and enzymatic activity of a positive Au NPs ((+) Au NPs)-based colorimetric immunoassay [60]. According to this study, antibody-modified (+) Au NPs possessed an activity similar to that of peroxidase, so this NP was used as an artificial enzyme instead of horseradish peroxidase (HRP) during the biosensing process. The reaction between (+) Au NPs and $H_2O_2$ induced the oxidation of 3,3',5,5'-tetramethylbenzidine (TMB), after which a blue color was observed because of the oxidized TMB ($TMB_{ox}$) [61]. The plasmonic absorbance of the (+) Au NPs was measured at approximately 526 nm, and the size of the NPs was determined to be approximately 50 nm. Colorimetric detection was demonstrated for several combinations of mixing components to prove the role of each material. A strong blue color with a wavelength of approximately 656 nm was observed only with the use of (+) Au NPs conjugated with a specific antibody against hemagglutinin (HA) (aB 66189), TMB and $H_2O_2$, and no color change occurred in the other conditions. This result indicated that the target virus was detected only in the presence of the suggested Au NPs, TMB and $H_2O_2$. The catalytic (+) Au NP-based colorimetric sensing

system showed excellent selectivity against other types of biomolecules and a high sensitivity with a low LOD (approximately 10.79 pg/ml).

Noble metal-based core/shell NPs could also play the role of an artificial enzyme. For example, He *et al.* reported the detection of interleukin-2 via a Au@Pt core/shell NP-based immunoassay [62]. In this case, Au@Pt NPs showed a better catalytic activity and stability than HRP, and this sensing system exhibited a low LOD of 12.5 pg/ml. In other studies, metal ions were utilized as artificial co-enzymes for enhancing the catalytic activity of Au NPs in colorimetric detection [63], and as a result, the sensitivity of the catalytic Au NP-based sensing platform was improved in the presence of metal ions [64-68]. In this case, metal ions and a mild reducing agent were added to the sensing solution after an antigen-antibody/Au NP conjugation process, in which the metal ions were reduced and the resulting metal covered the surface of the Au NPs [63, 67]. This core-shell structure exhibited an enhanced detection performance since the new metal layer formed on the Au NPs was exposed to and in direct contact with the medium without hindrance by antibodies or biomolecules, so this new bare metal surface showed enhanced catalytic activity [69, 70].

With the various strategies described above, several plasmonic and catalytic NP-based detection platforms have been developed and introduced to contribute to public health and the protection against harmful biomolecules.


## 3. Fluorescent QDs for biosensing systems

Engineered inorganic or organic fluorescent QDs have been frequently applied as signal indicators in biosensing systems [71-74]. In particular, the fluorescence intensity or properties of QDs can be tuned through interactions with other types of NPs or CNMs, and interesting synergistic properties can be obtained, such as PRET and fluorescence (or Förster) resonance energy transfer (FRET) [25, 75, 76]. Based on these kinds of synergistic properties, several types of highly sensitive and selective fluoroimmunoassay (FI) has been developed for the detection of biomolecules and infectious viruses.

The fluorescence intensity of QDs is enhanced by the PRET phenomenon that occurs via interaction between QDs and plasmonic NPs or CNMs [77]. In this case, the collective effect in a hybrid structure consisting of plasmonic materials and fluorescent nanoparticles enhances the fluorescence [78]. To detect viruses, DNA, RNA and biomolecules, PRET-based FIs have been developed by using several plasmonic nanomaterials, including MeNPs, core/shell NPs, MeNP-CNMs, inorganic QDs, carbon dots and GRP-QDs [79-83].

Takemura *et al.* reported the detection of influenza virus through the PRET effect by using urchin-like Au NPs (u-Au NPs) and inorganic CdSeTeS QDs (Figure 3) [84]. In this system, the u-Au NPs were utilized as a plasmonic substrate for energy transfer, while the QDs acted as the fluorescence indicator and captured the target influenza virus. A specific antibody was introduced on the surface of both NPs, and when the target virus was present in the sensing solution, the two types of NPs assembled via an antigen and antibody conjugation process to form a hybrid structure. Subsequently, virus-mediated plasmon energy transfer from the u-Au NPs to the QDs occurred. Finally, the fluorescence intensity of the QDs was enhanced in the presence of the virus, and the enhancement in the intensity was correlated with the amount of virus (Figure 3A). The PRET-based FI for the influenza virus was successfully demonstrated, and its sensitivity was characterized in deionized (DI) water and a human serum environment (Figure 3B and C). The fluorescence enhancement was clearly observed in both systems depending on the concentration of influenza virus, and the fluorescence enhancement factor (fluorescence intensity after PRET-FI /fluorescence intensity of the initial state = $F/F_0$) linearly increased with increasing amount of influenza (Figure 3D). The sensitivity in human serum was lower than that in DI water due to protein interruption; however, reasonable detection results were obtained with a low LOD of approximately 0.03 pg/ml in DI water and approximately 0.4 pg/ml in human serum.

Recently, dengue virus RNA was detected through a PRET-based FI by using a Au NP-alloyed QD hybrid structure with a molecular beacon (MB) [71]. In this study, the sensing structure was designed so that one side of the hairpin-structured MB was conjugated with a fluorescence quencher, while the other side of the structure was combined with an Au NP-alloyed

QD hybrid structure. Therefore, before hybridization between the target RNA and MB, the fluorescence intensity of the QDs was too weak due to the presence of an adjacent quencher, even though the QDs were conjugated with Au NPs. However, when the target RNA was present in the sensing system, the loop part of the MB hybridized, and the hairpin structure of the MB changed to a linear structure. Finally, the fluorescence intensity of the QDs could be recovered by separation from the neighboring Au NPs, and the fluorescence enhancement factor was correlated with the amount of target RNA. The detection of various concentrations of dengue virus RNA was carried out, and a high sensitivity was shown with a low LOD of approximately 20 copies/ml.

MeNP-decorated GRP or CNT (MeNP-GRP or MeNP-CNT) was also applied as a plasmonic substrate for the detection of viruses by PRET. GRP and CNTs possess pi electrons, so they can also have plasmonic properties, and plasmonic coupling can thus occur with the MeNPs located on the surface of GRP or CNTs.

Lee *et al.* reported the detection of influenza virus via Au NP-CNT- and QD-based PRET FIs [85]. In this study, Au NPs were introduced on the surface of CNTs via a facile 2-step process in DI water at room temperature. The Au-CNT structure was observed by TEM (Figure 4A). The Au NP-CNTs played the role of a plasmonic substrate and induced an enhancement in the fluorescence of the QDs in the presence of influenza virus (H1N1). A specific antibody was introduced on the surface of the Au-CNTs and QDs via an ethyl(dimethylaminopropyl) carbodiimide/N-hydroxysuccinimide (EDC/NHS) coupling reaction. The fluorescence enhancement of the QDs was monitored in the presence of various concentrations of influenza virus and clinically isolated influenza virus to demonstrate the sensitivity of the system. According to Figure 4B and C, the fluorescence intensity of the QDs in the presence of influenza virus and the clinical sample gradually increased as the amount of target virus increased and showed a high sensitivity and a linear response. The LODs of influenza virus and the isolated real sample were 0.1 pg/ml and 50 PFU/ml, respectively.

The detection of the influenza virus was also accomplished by using Au-CNTs and QDs. When the virus was present in the sensing solution, a sandwich structure formed between the Au-CNTs and QDs via an antibody and antigen conjugation process, and as a result, green fluorescence was observed from the CNT structure (Figure 4D and F). Additionally, Au NP-GRP has been used as a plasmonic substrate in a PRET-based FI to monitor the tuberculosis antigen CFP-10 [82]. In this case, Au NP-GRP and CdTe QDs were modified with anti CFP-10 aB to induce the formation of an antigen-mediated sandwich structure, and the fluorescence enhancement of the QDs was measured in the presence of various CFP-10 concentrations to demonstrate the PRET-based FI. This approach showed highly sensitive detection with an estimated LOD of approximately 4.5 pg/ml. In addition, high selectivity against other types of tuberculosis antigens was observed.

FRET-based FIs have also been investigated for biosensing platforms [86-90]. The FRET effect is a unique and interesting optical phenomenon that occurs between different types of fluorescent materials that possess different bandgap energies for fluorescence irradiation [91-93]. In this case, energy transfer takes place from the higher bandgap energy to the lower bandgap energy through dipole-dipole interactions within the range of approximately 10 nm [94].

The leukemia-related cDNA was detected by using Cadmium telluride (CdTe) QDs and methylene blue via a FRET-based FI [95]. CdTe NP is well known semiconductor fluorescent nanomaterial, which was composed of cadmium and tellurium. Shamsipur *et al.* reported the modification of a QD surface with probe DNA to capture the target cDNA, and after DNA hybridization between the target and probe DNA, methylene blue automatically adhered to and intercalated between the hybridized double DNA strain. After this process, energy transfer occurred from the CdTe QDs to methylene blue, and subsequently, the fluorescence intensity of methylene blue at approximately 700 nm increased while that of QD at 599 nm decreased due to the FRET effect. In addition, the intensity of fluorescence of methylene blue was changed in the presence of various concentrations of target DNA. In this case, the LOD was calculated from the increasing ratio of the fluorescence intensity of the methylene blue-based calibration curve to be

11

0.15 nM. Similarly, Bhuckory *et al.* demonstrated a PRET-based FI for the detection of prostate specific antigen by using QDs and Lumi4Tb [96]. In this case, the donor was Lumi4Tb, and the acceptor was QDs. After the antibody-antigen conjugation process, the fluorescence intensity of the QD was measured to obtain the calibration curve. The sensitivity showed an LOD of approximately 4 ng/ml.

The FRET effect also causes quenching of the fluorescence of QDs [97]. In this case, energy transfer occurs between QDs and MeNPs or a CNM [98-100]. As mentioned above, the surface plasmon resonance absorbs light energy at a certain wavelength, so the irradiated fluorescence energy could also be absorbed by the counter nanomaterials, resulting in a decrease in the fluorescence intensity through quenching. Therefore, the target could be detected through a target biomolecule-mediated quenching process [101, 102]. Furthermore, if the nanomaterials were removed or placed farther from the QDs by target biomolecules after the quenching process, the fluorescence intensity could be recovered, and this strategy could be applied in a biosensing process [103-105].

Shi and co-workers demonstrated the detection of the mecA gene that is resistant to antibiotics [106], using GQDs and Au NPs via a FRET-based quenching process [102]. The GQDs and Au NPs were modified with probe DNAs, and both NPs were conjugated with target DNA via DNA hybridization. In this case, because the emission wavelength of the GQDs was approximately 460 nm and the plasmonic absorbance wavelength of the Au NPs was approximately 520 nm, the wavelengths overlapped, and as a result, energy transfer occurred between the GQDs and Au NPs. In other words, because the fluorescence energy from the GQDs was absorbed the by Au NPs, fluorescence quenching occurred. As the amount of target DNA increased, more GQDs were conjugated with Au NPs, and the fluorescence intensity decreased further due to the FRET-based quenching effect. Based on this concept, the researchers calculated the quenching yield from various concentrations of the target DNA. In this case, almost 85 % of the fluorescence signal was quenched by approximately 100 nM mecA gene, and the detection limitation of this biosensing system was 1 nM.

In the other studies, the upconversion nanoparticles (UCNPs) were utilized as fluorescence donor in the FRET-based biosensing system [100, 107, 108]. Normally, lanthanide or actinide doped transitional metal structures played as UCNPs, and FI was demonstrated through the energy transfer from UCNP to specific fluorescence acceptor. UCNPs-based FI showed high sensitivity and selectivity. For example, Wu et al., had detected carcinoembryonic antigen (CEA) by using NaYF4:Yb:Er-based UCNP [108]. In this study, fluorescence acceptor was carbon nanoparticle (CNP). This UCNP was coated with poly acrylic acid (PAA) and then it was modified with CEA aptamer. Subsequently, CNP was anchored with CEA aptamer which was on the PAA-UCNP in order to induce the FRET-based quenching of UCNP, then the fluorescence of UCNP was decreased by CNP. However, when the CEA was introduced to this hybrid system, the fluorescence of UCNP was recovered because the CNP was released from the UCNP due to the higher binding affinity between CEA and CEA aptamer than between CNP and CEA aptamer. The recovery rate of fluorescence of UCNP was dependent on the concentration of CEA. The linear response was obtained in the range from 0.1 to 40 ng/ml CEA concentration and high sensitivity was shown by sensitivity test for CEA.

## 4. Nanoparticle-functionalized CNTs and GRP-based electrical and optical biosensing systems

CNMs, including CNT and GRP, possess a high electrical conductivity and superior mechanical properties, so these nanomaterials can be applied in various sensing fields. In addition, NP-CNMs also have been of interest due to their improved and synergistic properties, such as their enhanced electrical conductivity, electrochemical properties and mechanical strength, and their SERS effect. Therefore, NP-CNMs have been widely utilized as electrical, electrochemical, flexible and wearable biosensors. Additionally, they have been applied in SERS-based biosensors.

Lee and co-workers introduced the detection of norovirus-like particles (NoV-LPs) using a binary NPs-GRP electrical sensing channel-based biosensing platform [109]. In this study, Au NPs and MNPs were introduced on the surface of GRP in DI water at room temperature. The

resulting modified GRP possessed multiple functionalities, such as magnetic, plasmonic, and electrical properties. To detect the NoV-LPs, Au/MNP-GRP was magnetically deposited on the surface of a Pt electrode to fabricate sensing channels, after which an anti-norovirus antibody was introduced on the surface of Au/MNP-GRP via an EDC/NHS coupling reaction. The electrical conductivity was measured after antibody conjugation and is represented as $R_0$. Subsequently, target NoV-LPs were introduced into the system, and the electrical conductivity ($R_{NoV-LP}$) was measured to determine the change in resistance in the presence of NoV-LPs. In this case, the resistance of the sensing channel increased after the addition of NoV-LPs into the sensing system, and as the concentration of NoV-LPs increased, the resistance of Au/MNP-GRP also linearly increased. The calibration curve was plotted by using the value of $\Delta R_{NoV-LP\ detection} = (R_{NoV-LP+aB} - R_{aB})/R_{aB}$ in the presence of various concentrations of NoV-LPs from 0.01 pg/ml to 1 ng/ml. The LOD was low with a value of approximately 1.16 pg/mL, and a high selectivity against other biomolecules was shown.

In addition, influenza DNA and norovirus DNA were detected by using Au/MNP-CNTs via a similar approach as in the Au/MNP-GRP case (Figure 5A) [110]. The Au/MNP-CNTs were magnetically aligned on the surface of a Pt interdigitated electrode (IDE), and then thiol-modified probe DNA specific for influenza or norovirus DNA was introduced on the surface of the Au/MNP-CNTs for utilization as electrical sensing channels. Without the application of a magnetic field, the hybrid structures were randomly located on the surface of the Pt IDE, but those structures were aligned with the application of a magnetic field, which clearly observed by SEM (Figure 5B and C). After modification of the Au/MNP-CNTs with probe DNA, the resistance of the hybrid sensing channel was measured to obtain the $R_{prb}$ value, and then DNA hybridization between the target and probe was conducted to demonstrate DNA sensing. The resistance of the sensing channel was also measured after the DNA hybridization process and is represented as $R_{hyb}$. The sensitivity of this system was calculated with the equation $\Delta R_{target\ detection} = (R_{hyb} - $

$R_{prb}$)/$R_{prb}$, and the Au/MNP-CNT-based DNA sensing system showed excellent sensitivity with an LOD of 8.4 pM for influenza virus DNA and approximately 8.8 pM for norovirus DNA.

NP-CNMs also strongly contributed to electrochemical biosensing platforms [111-114]. Liu *et al.* reported that hepatitis B virus genomic DNA (HBV-DNA) was successfully detected by using tungsten disulfide (WS$_2$)-multiwalled CNT (MWCNT) through an electrochemical biosensing system [115]. The WS$_2$ is well known as semiconducting transition metal/dichalcogenides material and it showed 2D inorganic structure. In this case, the researchers prepared a glassy carbon electrode (GCE) with WS$_2$-MWCNTs, and then Au NPs were introduced on this modified hybrid structure to immobilize the probe DNA on the Au-WS$_2$-MWCNT-GCE structure. When the target virus was present in this system, hybridization occurred, so the target DNA was conjugated to the surface of the electrode. After that, the researchers used auxiliary DNA as a linker to induce a hybridization chain reaction between the target DNA and biotin-avidin-HRP for amplification of the electrochemical signal. The amount of the HRP-based complex structure was determined by the amount of target DNA, so the electrochemical signal of hydroquinol oxidation catalyzed by HRP with H$_2$O$_2$ was correlated with the target DNA concentration. The electrochemical signal of catalytic hydroquinol oxidation on the HRP-Au-WS$_2$-MWCNT-GCE was measured by differential pulse voltammetry (DPV) in the presence of various concentrations of the target HBV virus DNA. The current decreased as the concentration of DNA increased, and the LOD was estimated to be approximately 2.5 fM.

By using NP-CNMs, a system that functioned not only as an electrical biosensor but also a SERS-based optical sensor was developed. Zheng and co-workers conducted mRNA detection by using AgNP-CNTs via a SERS-based biosensor [116]. In this study, single-stranded DNA was introduced onto CNTs to conjugate Ag NPs on the CNT and prepare a SERS-active substrate. In addition, the researchers detected miR-21 mRNA, which is a potential cancer marker. After interaction between miR-21 and the Ag NP-CNTs, an enhanced Raman signal was collected at approximately 1605 cm$^{-1}$. In this case, the Raman intensity increased as the target mRNA concentration increased, and excellent sensitivity was obtained for various concentrations of miR-

21. The LOD was estimated to be approximately 5 pM, and a high selectivity against other types of miRNA was observed for this sensing system. Together, these reports show that these multifunctional hybrid carbon nanomaterials can be applied as signal transducers for various types of biosensors.

## 5. Conclusions

In order to detect dangerous and infectious diseases and to develop the effective diagnosis, many kinds of nanomaterials have been utilized for high-performance biosensors. In addition, based on their properties and functionalities, various detection techniques have also been investigated for the development of novel biosensing platforms. Several biomolecules, such as viruses, antigens, DNA, RNA and proteins, have been successfully detected and monitored by using NP-, CNM-, and hybrid nanomaterial-based biosensors through signal transduction of optical, electrical, and electrochemical sensing signals. Therefore, nanomaterial-based biosensors were shown to exhibit good potential for application in promising detection systems, which will be beneficial for public health and society.

## Conflict of interest

The authors declare no financial or commercial conflict of interest.

## References

[1] Syedmoradi, L., Daneshpour, M., Alvandipour, M., Gomez, F. A*., et al.*, *Biosens. Bioelectron.* **2017**, *87*, 373.

[2] Darwish, N. T., Sekaran, S. D., Khor, S. M., *Sens. Actuator B-Chem.* **2018**, *255*, 3316.

[3] Wang, Y., Yu, L., Kong, X., Sun, L., *Int. J. Nanomed.* **2017**, *12*, 4789.

[4] Hill, R. T., *Wiley Interdiscip. Rev.-Nanomed. Nanobiotechnol.* **2015**, *7*, 152.

[5] Spackova, B., Wrobel, P., Bockova, M., Homola, J., *Proc. IEEE* **2016**, *104*, 2380.

[6] Walcarius, A., Minteer, S. D., Wang, J., Lin, Y., Merkoci, A., *J. Mater. Chem. B* **2013**, *1*, 4878.

[7] Song, Y., Wei, W., Qu, X., *Adv. Mater.* **2011**, *23*, 4215.

[8] Gao, C., Lu, Z., Liu, Y., Zhang, Q., Chi, M., Cheng, Q., Yin, Y., *Angew. Chem.-Int. Edit.* **2012**, *51*, 5629.

[9] Hu, M., Chen, J., Li, Z.-Y., Au, L., Hartland, G.V., Li, X, Marquez, M., Xia, Y., *Chem. Soc. Rev.* **2006**, *35*, 1084.

[10] Pattnaik, S., Swain, K., Lin, Z., *J. Mater. Chem. B* **2016**, *4*, 7813.

[11] Liu, H., Zhang, L., Yan, M., Yu, J., *J. Mater. Chem. B* **2017**, *5*, 6437.

[12] Bruchez, M., Moronne, M., Gin, P., Weiss, S., Alivisatos, A. P., *Science* **1998**, *281*, 2013.

[13] Medintz, I. L., Uyeda, H. T., Goldman, E. R., Mattoussi, H., *Nat. Mater.* **2005**, *4*, 435.

[14] Lin, Y., Ren, J., Qu, X., *Accounts Chem. Res.* **2014**, *47*, 1097.

[15] Suzuki, N., Wang, Y., Elvati, P., Qu, Z.-b., Kim, K., Jiang, S., Baumeister, E., Lee, J., Yeom, B., Bahng, J.H., Lee, J, Violi, A., Kotov, N.A., *ACS Nano* **2016**, *10*, 1744.

[16] Lee, J., Kim, H. Y., Zhou, H., Hwang, S., Koh, K., Han, D.W., Lee, J., *J. Mater. Chem.* **2011**, *21*, 13316.

[17] Lee, J., Lee, J., *Chem. Commun.* **2017**, *53*, 5814.

[18] Lee, J., Lee, K., Park, S. S., *J. Mater. Sci.* **2016**, *51*, 2761.

[19] Lee, J., Mulmi, S., Thangadurai, V., Park, S. S., *ACS Appl. Mater. Interfaces* **2015**, *7*, 15506.

[20] Mayani, V. J., Mayani, S. V., Kim, S. W., *Sci. Rep.* **2017**, *7*, 7239.

[21] Jeong, M.-S., Ahn, D.-R., *Analyst* **2015**, *140*, 1995.

[22] H. R, C., Schiffman, J. D., Balakrishna, R. G., *Sens. Actuator B-Chem.* **2018**, *258*, 1191.

[23] Li, R. S., Yuan, B., Liu, J. H., Liu, M. L., Gao, P. F., Li, Y. F., Li, M., Huan, C. Z., *J. Mater. Chem. B* **2017**, *5*, 8719.

[24] Moraes Silva, S., Tavallaie, R., Sandiford, L., Tilley, R. D., Gooding, J. J., *Chem. Commun.* **2016**, *52*, 7528.

[25] Lee, J., Takemura, K., Park, E., *Sensors* **2017**, *17*, 2332.

[26] Park, J. E., Kim, K., Jung, Y., Kim, J. H., Nam, J. M., *ChemNanoMat* **2016**, *2*, 927.

[27] Maduraiveeran, G., Sasidharan, M., Ganesan, V., *Biosens. Bioelectron.* **2018**, *103*, 113.

[28] Zhu, Z., *Nano-Micro Lett.* **2017**, *9*, 25.

[29] Rabti, A., Raouafi, N., Merkoçi, A., *Carbon* **2016**, *108*, 481.

[30] Zhang, S., Geryak, R., Geldmeier, J., Kim, S., Tsukruk, V. V., *Chem. Rev.* **2017**, *117*, 12942.

[31] Xi, J., Xie, C., Zhang, Y., Wang, L., Xiao, J.,Duan, X., Ren, J., Xiao, F., Wang, S., *ACS Appl. Mater. Interfaces* **2016**, *8*, 22563.

[32] Ahmed, S. R., Takemeura, K., Li, T.-C, Kitamoto, N., Tanaka, T., Suzuki, T., Park, E. Y., *Biosens. Bioelectron.* **2017**, *87*, 558.

[33] Kim, J., Jang, M., Lee, K. G., Lee, K.-S., Lee, S.J., Ro, K.-W., Kang, I.S., Do Jeong, B., Park, T.J., Kim, H.-J. Lee, J., *ACS Appl. Mater. Interfaces* **2016**, *8*, 23489.

[34] Lee, J., Zhou, H., Lee, J., *J. Mater. Chem.* **2011**, *21*, 16935.

[35] Oh, S., Jang, M., Kim, J., Lee, J., Zhou, H., Lee, J., *Curr. Appl. Phys.* **2016**, *16*, 738.

[36] Sabela, M., Balme, S., Bechelany, M., Janot, J. M., Bisetty, K., *Adv. Eng. Mater.* **2017**, *19*, 1700270.

[37] Wu, M., Kuga, S., Huang, Y., *Langmuir* **2008**, *24*, 10494.

[38] Sawitowski, T., Miquel, Y., Heilmann, A., Schmid, G., *Adv. Funct. Mater.* **2001**, *11*, 435.

[39] Lin, S., Li, M., Dujardin, E., Girard, C., Mann, S., *Adv. Mater.* **2005**, *17*, 2553.

[40] Chen, T., Hong, Y., Reinhard, B. M., *Nano Lett.* **2015**, *15*, 5349.

[41] Ding, B., Deng, Z., Yan, H., Cabrini, S., Zuckermann, R.N., Bokor, J., *J. Am. Chem. Soc.* **2010**, *132*, 3248.

[42] Schreiber, R., Santiago, I., Ardavan, A., Turberfield, A. J., *ACS Nano* **2016**, *10*, 7303.

[43] de la Rica, R., *Nanoscale* **2017**, *9*, 18855.

[44] Hamedi, M., Wigenius, J., Tai, F.-I., Bjork, P., Aili, D., *Nanoscale* **2010**, *2*, 2058.

[45] Saha, K., Agasti, S. S., Kim, C., Li, X., Rotello, V. M., *Chem. Rev.* **2012**, *112*, 2739.

[46] Yang, X., Gao, Z., *Chem. Commun.* **2015**, *51*, 6928.

[47] Zhang, T., Li, H., Hou, S., Dong, Y., Pang, G., Zhane, Y., *ACS Appl. Mater. Interfaces* **2015**, *7*, 27131.

[48] Guo, L., Xu, Y., Ferhan, A. R., Chen, G., Kim, D.-H., *J. Am. Chem. Soc.* **2013**, *135*, 12338.

[49] Kim, J., Lee, K.-S., Kim, E. B., Paik, S., Chang, C.L., Park, T.J. Kim, H.-J., Lee, J., *Biosens. Bioelectron.* **2017**, *96*, 68.

[50] Tran, V. T., Kim, J., Tufa, L. T., Oh, S., Kwon, J., Lee, J., *Anal. Chem.* **2018**, *90*, 225.

[51] Kim, J., Lee, J., Lee, K.-I., Park, T. J., Kim, H.-J., Lee, J., *Sens. Actuator B-Chem.* **2013**, *177*, 327.

[52] Ambrosi, A., Airò, F., Merkoçi, A., *Anal. Chem.* **2010**, *82*, 1151.

[53] Zhan, L., Wu, W. B., Yang, X. X., Huang, C. Z., *New J. Chem.* **2014**, *38*, 2935.

[54] Gao, L., Zhuang, J., Nie, L., Zhang, J., Zhang, Y., Gu, N., Wang, T., Feng, J., Yang, D., Perrett, S., Yan, X., *Nat. Nanotechnol.* **2007**, *2*, 577.

[55] Cao-Milan, R., He, L. D., Shorkey, S., Tonga, G. Y., Wang, L.-S., Zhang, X., Uddin, I., Das, R., Sulak, M., Rotello, V. M*., Mol. Syst. Des. Eng.* **2017**, *2*, 624.

[56] Wei, H., Chen, C., Han, B., Wang, E., *Anal. Chem.* **2008**, *80,* 7051.

[57] Sloan-Dennison, S., Laing, S., Shand, N. C., Graham, D., Faulds, K., *Analyst* **2017**, *142*, 2484.

[58] Peng, M.-P., Ma, W., Long, Y.-T., *Anal. Chem.* **2015**, *87*, 5891.

[59] Oh, S., Kim, J., Tran, V. T., Lee, D. K., Ahmed, S.R., Hong, J.C., Lee, J., Park, E.Y., Lee, J., *ACS Appl. Mater. Interfaces* **2018,** *10,* 12534.

[60] Ahmed, S. R., Kim, J., Suzuki, T., Lee, J., Park, E. Y., *Biotechnol. Bioeng.* **2016**, *113*, 2298.

[61] Jv, Y., Li, B., Cao, R., *Chem. Commun.* **2010**, *46*, 8017.

[62] He, W., Liu, Y., Yuan, J., Yin, J.-J., Wu, X., Hu, X., Zhang, K., Liu, J., Chen, C., Ji, Y., Guo, Y., *Biomaterials* **2011**, *32*, 1139.

[63] Liang, R.-Q., Tan, C.-Y., Ruan, K.-C., *J. Immunol. Methods* **2004**, *285*, 157.

[64] Kim, G. B., Lee, J. O., Kim, Y.-P., *Sens. Actuator B-Chem.* **2017**, *246*, 271.

[65] Liu, R., Zhang, Y., Zhang, S., Qiu, W., Gao, Y., *Appl. Spectrosc. Rev.* **2014**, *49*, 121.

[66] Liu, R., Liu, X., Tang, Y., Wu, L., Hou, X., Lv, Y*., Anal. Chem.* **2011**, *83*, 2330.

[67] Gupta, S., Huda, S., Kilpatrick, P. K., Velev, O. D., *Anal. Chem.* **2007**, *79*, 3810.

[68] He, H., Xu, X., Wu, H., Jin, Y., *Adv. Mater.* **2012**, *24*, 1736.

[69] Liu, Y., Xie, J., Zhang, Z., Lu, Z., *RSC Adv.* **2016**, *6*, 89484.

[70] Wang, S., Chen, Z., Choo, J., Chen, L., *Anal. Bioanal. Chem.* **2016**, *408*, 1015.

[71] Adegoke, O., Park, E. Y., *J. Mater. Chem. B* **2017**, *5*, 3047.

[72] Adegoke, O., Seo, M.-W., Kato, T., Kawahito, S., Park, E. Y., *J. Mater. Chem. B* **2016**, *4*, 1489.

[73] Sun, L., Li, S., Ding, W., Yao, Y., Yang, X., Yao, C., *J. Mater. Chem. B* **2017**, *5*, 9006.

[74] Chan, W. C. W., Nie, S., Q, *Science* **1998**, *281*, 2016.

[75] Zeng, Q., Zhang, Y., Liu, X., Tu, L., Kong, X., Zhang, H., *Chem. Commun.* **2012**, *48*, 1781.

[76] Shi, J., Tian, F., Lyu, J., Yang, M., *J. Mater. Chem. B* **2015**, *3*, 6989.

[77] Lee, J., Hernandez, P., Lee, J., Govorov, A. O., Kotov, N. A., *Nat. Mater.* **2007**, *6*, 291.

[78] Lee, J., Govorov, A. O., Dulka, J., Kotov, N. A., *Nano Lett.* **2004**, *4*, 2323.

[79] Ashiba, H., Sugiyama, Y., Wang, X., Shirato, H., Higo-Moriguchi, K., Taniguchi, K., Ohki, Y., Fujimaki, M., *Biosens. Bioelectron.* **2017**, *93*, 260.

[80] Adegoke, O., Morita, M., Kato, T., Ito, M., Suzuki, T., Park, E.Y., *Biosens. Bioelectron.* **2017**, *94*, 513-522.

[81] Zou, F., Zhou, H., Tan, T. V., Kim, J., Koh, K., Lee, J., *ACS Appl. Mater. Interfaces* **2015**, *7*, 12168.

[82] Lee, J., Kim, J., Ahmed, S. R., Zhou, H., Kim, J.-M., Lee, J., *ACS Appl. Mater. Interfaces* **2014**, *6*, 21380.

[83] Ahmed, S. R., Hossain, M. A., Park, J. Y., Kim, S.-H., Lee, D., Suzuki, T., Lee, J., Park, E.Y., *Biosens. Bioelectron.* **2014**, *58*, 33.

[84] Takemura, K., Adegoke, O., Takahashi, N., Kato, T., Li, T.-C., Kitamoto, N., Tanaka, T., Suzuki, T., Park, E.Y., *Biosens. Bioelectron.* **2017**, *89*, 998.

[85] Lee, J., Ahmed, S. R., Oh, S., Kim, J., Suzuki, T., Parmar, K., Park, S.S., Lee, J., Park, E.Y., *Biosens. Bioelectron.* **2015**, *64*, 311-317.

[86] Tian, J., Wei, W., Wang, J., Ji, S., Chen, G., Lu, J., *Anal. Chim. Acta* **2018**, *1000*, 265.

[87] Li, H., Shi, L., Sun, D.-e., Li, P., Liu, Z., *Biosens. Bioelectron.* **2016**, *86*, 791.

[88] Tian, J., Zhao, H., Liu, M., Chen, Y., Quan, X., *Anal. Chim. Acta* **2012**, *723*, 83.

[89] Wang, X., Lou, X., Wang, Y., Guo, Q., Fang, Z., Zhong, X., Mao, H., Jin, Q., Wu, L., Zhao, H., Zhao, J., *Biosens. Bioelectron.* **2010**, *25*, 1934.

[90] Hu, J., Wang, Z.-y., Li, C.-c., Zhang, C.-y., *Chem. Commun.* **2017**, *53*, 13284.

[91] Clapp, A. R., Medintz, I. L., Mattoussi, H., *ChemPhysChem* **2006**, *7*, 47.

[92] Hildebrandt, N., Spillmann, C. M., Algar, W. R., Pons, T., Stewart, M.H., Oh, E., Susumu, K., Diaz, S.A., Delehanty, J.B., Medintz, I.L., *Chem. Rev.* **2017**, *117*, 536.

[93] Stanisavljevic, M., Krizkova, S., Vaculovicova, M., Kizek, R., Adam, V., *Biosens. Bioelectron.* **2015**, *74*, 562.

[94] Algar, W. R., Ancona, M. G., Malanoski, A. P., Susumu, K., Medintz, I. L., *ACS Nano* **2012**, *6*, 11044.

[95] Shamsipur, M., Nasirian, V., Barati, A., Mansouri, K., Vaisi-Raygani, A., Kashanian, S., *Anal. Chim. Acta*, *966*, 62-70.

[96] Bhuckory, S., Lefebvre, O., Qiu, X., Wegner, K., Hildebrandt, N., *Sensors* **2016**, *16*, 197.

[97] Samanta, A., Zhou, Y., Zou, S., Yan, H., Liu, Y., *Nano Lett.* **2014**, *14*, 5052.

[98] Haldar, K. K., Sen, T., Patra, A., *J. Phys. Chem. C* **2010**, *114*, 4869.

[99] Chang, L., He, X., Chen, L., Zhang, Y., A *Nanoscale* **2017**, *9*, 3881.

[100] Alonso-Cristobal, P., Vilela, P., El-Sagheer, A., Lopez-Cabarcos, E., Brown, T., Muskens, O.L., Rubio-Retama, J., Kanaras, A.G., *ACS Appl. Mater. Interfaces* **2015**, *7*, 12422.

[101] Fu, Y., Chen, T., Wang, G., Gu, T., Xie, C., Huang, J., Li, X., Best, S., Han, G., *J. Mater. Chem. B* **2017**, *5*, 7133.

[102] Shi, J., Chan, C., Pang, Y., Ye, W., Tian, F., Lyu, J., Zhang, Y., Yang, M., *Biosens. Bioelectron.***2015**, *67*, 595.

[103] Qaddare, S. H., Salimi, A., *Biosens. Bioelectron.* **2017**, *89*, 773.

[104] Zhao, H., Chang, Y., Liu, M., Gao, S., Yu, H., Quan, X., *Chem. Commun.* **2013**, *49*, 234.

[105] Dubertret, B., Calame, M., Libchaber, A. J., *Nat. Biotechnol.* **2001**, *19*, 365.

[106] Xu, Z., Shah, H. N., Misra, R., Chen, J., Zhang, W., Liu, Y., Cutler, R.R., Mkrtchyan, H.V., *Antimicrob. Resist. Infect. Control* **2018**, *7*, 73.

[107] Wang, G., Fu, Y., Ren, Z., Huang, J., Best,S., Li, X., Han, G., *Chem. Commun.* **2018**, *54*, 6324.

[108] Wu, Z., Li, H., Liu, Z., *Sens. Actuator B-Chem.* **2015**, *206*, 531.

[109] Lee, J., Takemura, K., Kato, C. N., Suzuki, T., Park, E. Y., *ACS Appl. Mater. Interfaces* **2017**, *9*, 27298.

[110] Lee, J., Morita, M., Takemura, K., Park, E. Y., *Biosens. Bioelectron.* **2018**, *102*, 425.

[111] Zhang, W., Li, F., Hu, Y., Gan, S., Han, D., Zhang, Q., Niu, L., *J. Mater. Chem. B* **2014**, *2*, 3142.

[112] Mahmoud, K. A., Hrapovic, S., Luong, J. H. T., *ACS Nano* **2008**, *2*, 1051.

[113] Song, W., Li, H., Liu, H., Wu, Z., Qiang, W., Xu, D., *Electrochem. Commun.* **2013**, *31*, 16.

[114] Wang, Y., Bai, X., Wen, W., Zhang, X., Wang, S., *ACS Appl. Mater. Interfaces* **2015**, *7*, 18872.

[115] Liu, X., Shuai, H.-L., Liu, Y.-J., Huang, K.-J., *Sens. Actuator B-Chem.* **2016**, *235*, 603.

[116] Zheng, J., Bai, J., Zhou, Q., Li, J., Li, Y., Yang, J., Yang, R., *Chem. Commun.* **2015**, *51*, 6552.

**Figure legend**

**Figure 1. Target DNA sensing performance by plasmonic coupling interaction between Au NPs.** A) Schematic illustration of the construction of target DNA-mediated self-assembly of Au NPs, B) difference in plasmonic properties between the core and core-satellite structures, and SEM images of C) the core particles and D) the DNA-mediated core-satellite hybrid structures.[47] Copyright (2015) American Chemical Society. E) Mechanism of target DNA-induced dimerization of Au NPs, F) dependence of the plasmonic absorbance spectrum on the target DNA concentration (numbers 1 to 6 represent 0, 1 pM, 10 pM, 100 pM, 1 nM, and 10 nM, respectively), G) sensitivity test and H) dimerized Au NP structure in the presence of 10 nM target DNA [48]. Copyright (2013) American Chemical Society.

**Figure 2. TB aG detection by magnetophoresis process with Au NPs and MNPs.** A) and B) Detection process of a magnetophoresis immunoassay for CFP-10 TB aG detection using Au NPs and MNPs, C) time-based plasmonic absorbance changes at 525 nm as a function of the magnetophoresis time for different CFP-10 concentrations and D) difference in absorbance monitored from 0 to $10^4$ pg/ml for a sensitivity test [51]. Copyright (2013) Elsevier.

**Figure 3. PRET-based FI with u-Au NPs and QDs**. A) Schematic illustration of the PRET-based FI process; fluorescence enhancement as a function of the virus concentration in B) DI water and C) human serum; and D) calibration curves in the two types of media [84]. Copyright (2017) Elsevier.

**Figure 4. Influenza virus detection via PRET based FI using Au-CNT and QDs.** A) TEM image of a Au-CNT and the sensitivity results for the detection of B) influenza virus and C) a clinically isolated influenza virus sample via PRET-based FI; confocal laser-scanning microscopy images of the influenza virus-mediated Au-CNT/QD hybrid structure: D) fluorescence image, E) differential interference contrast (DIC) image and F) merged image [85]. Copyright (2015) Elsevier.

**Figure 5. Hybrid nanomaterials based electrical biosensing platform.** A) Illustration of the magnetic alignment of Au/MNP-CNTs on a Pt IDE and SEM images of the Au/MNP-CNTs B) without magnetic field deposition and C) aligned with a magnetic field [110]. Copyright (2018) Elsevier.

*Short CV and photos (2 authors max, with the exception of articles with 3 authors – then please include all author photos and CV)*

**Dr. Jaewook Lee** is current researcher in Research Institute of Green Science and Technology, Shizuoka University. He received his BS degree in chemistry in 2007 and MS degree in Analytical chemistry in 2009 from Dongguk University, Korea. Dr. Lee earned his Ph.D. degree in Nano Fusion Technology from Pusan National University. His current research interest includes synthesis of multi-functional nanomaterials and sensor applications. He has also interested in nanoparticles decorated carbon nanomaterials for nano-optics, and surface modification of nanocomposites for biocompatibility and biodegradability in nano bio-medical applications.

**Dr. Enoch Y. Park** is currently a professor in Research Institute of Green Science and Technology, Shizuoka University. He received his MS degree in Korea Advanced Institute of Science and Technology in 1982, and Ph.D. degree in a major of Chemical Engineering from the University of Tokyo, Japan in 1990, and worked as assistant professor in the Department of Chem. Eng. Nagoya University for two years. He is currently interested in preparation and engineering of nanobiomaterials such as virus-like particles in silkworm larvae and their applicability on vaccine. Also, his research is focused on ultrasensitive detection of infectious viruses using nanomaterials.
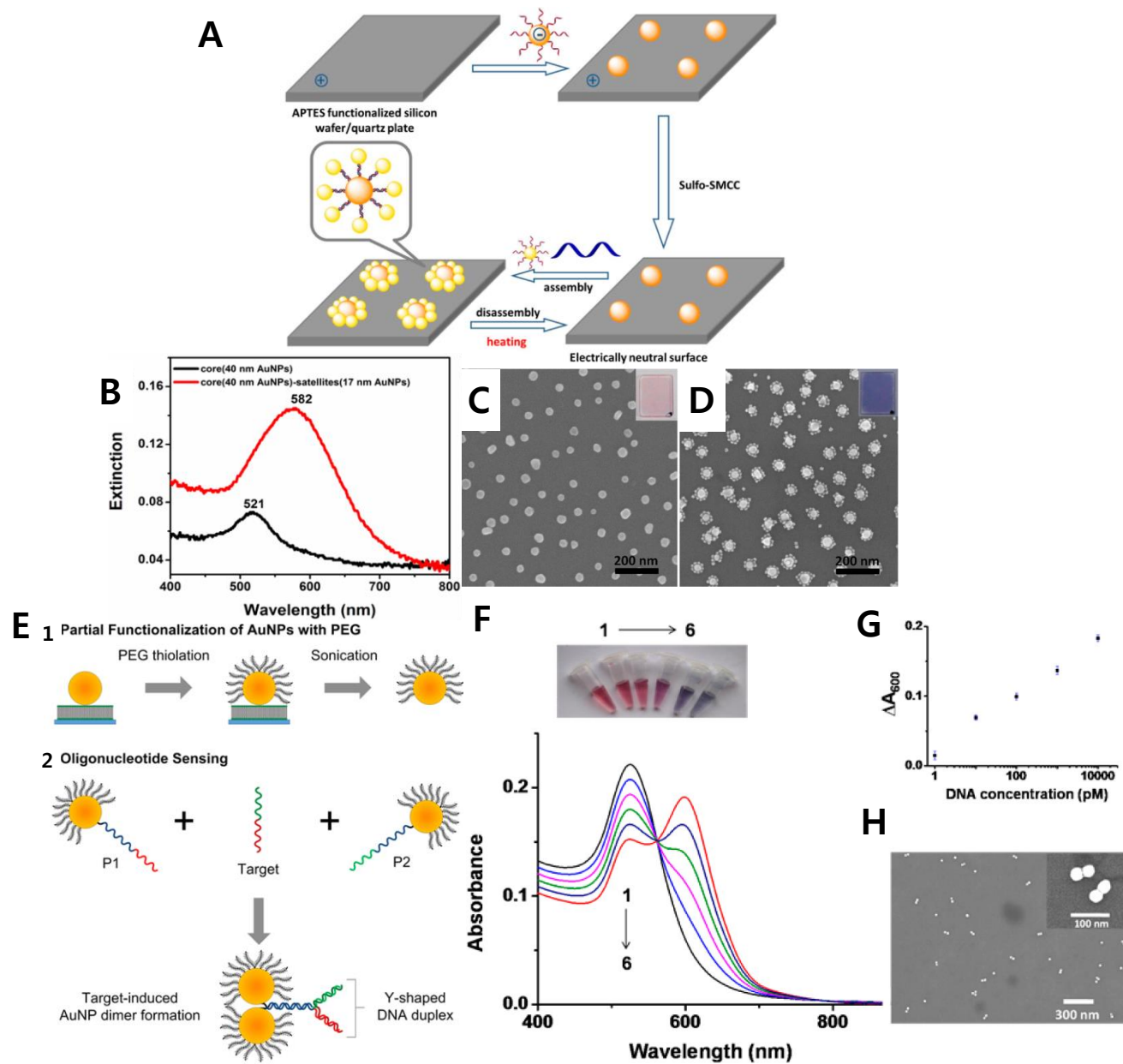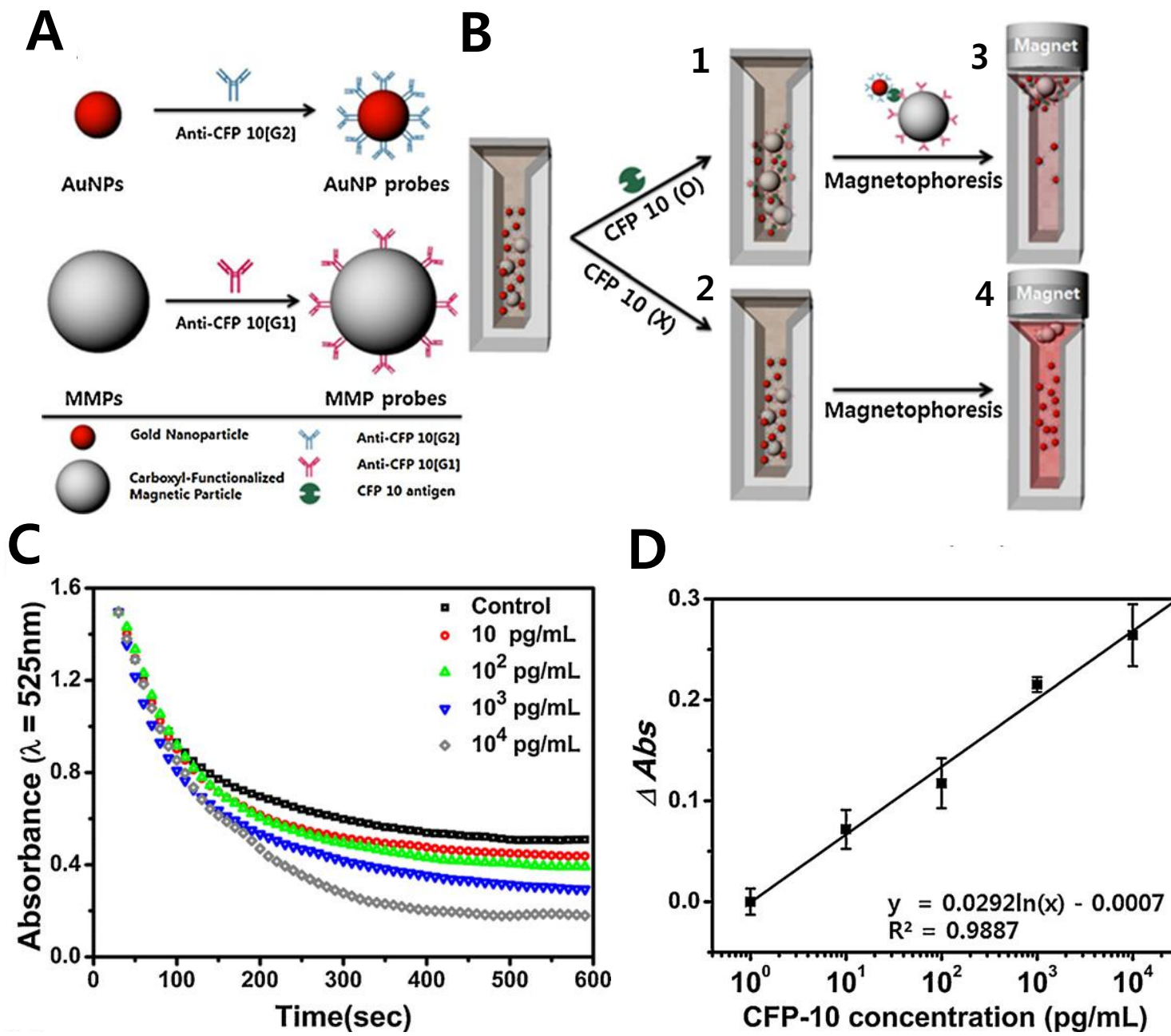
# Figure 1

# Figure 2



**A**

AuNPs → Anti-CFP 10[G2] → AuNP probes

MMPs → Anti-CFP 10[G1] → MMP probes

- ● Gold Nanoparticle
- ○ Carboxyl-Functionalized Magnetic Particle
- ⊥ Anti-CFP 10[G2]
- ⊥ Anti-CFP 10[G1]
- ● CFP 10 antigen

**B**

CFP 10 (O) → 1 → Magnetophoresis → 3 → Magnet

CFP 10 (X) → 2 → Magnetophoresis → 4 → Magnet

**C**

Absorbance ($\lambda$ = 525nm) vs Time(sec)

- ■ Control
- ○ 10 pg/mL
- △ $10^2$ pg/mL
- ▽ $10^3$ pg/mL
- ◇ $10^4$ pg/mL

**D**

$\triangle Abs$ vs CFP-10 concentration (pg/mL)

$y = 0.0292\ln(x) - 0.0007$
$R^2 = 0.9887$

# Figure 3

# Figure 4



A

100 nm

B

PL Intensity (x 10$^4$)

$y = 307.92\ln(x) + 10320$
$R^2 = 0.9842$

Virus Concentration (ng/ml)

C

Fluorescent intensity

Fluorescent intensity

Virus Concentration ( x 100 PFU/mL)

Virus Concentration (100 x PFU/mL)

D

2 µm

E

2 µm

F

2 µm

# Figure 5



A   AuNP   MNP   MWCNT   Au/MNP-CNT

Solution (Au/MNP-CNT)

Magnet     Magnet

Magnetic deposition

Magnetically aligned
Au/MNP-CNT on Pt-IDE
for DNA sensing channels

B

20 μm

C

20 μm